J. Plasma Physics (1998), *vol.* 59, *part* 2, *pp.* 277–302. Printed in the United Kingdom

Dynamics of hot filaments in a tokamak plasma

H. DE STERCK,[1] S. POEDTS[1] and J. P. GOEDBLOED[2]

[1]Centre for Plasma Astrophysics, Katholieke Universiteit Leuven, B-3001 Heverlee, Belgium

[2]FOM–Institute for Plasma Physics 'Rijnhuizen', PO Box 1207, 3430 BE Nieuwegein, The Netherlands

(Received 13 January 1997 and in revised form 11 August 1997)

The reaction of an equilibrium tokamak plasma to a sudden localized deposition of heat is investigated by means of numerical simulations of the time-dependent equations of resistive magnetohydrodynamics (MHD) in two spatial dimensions, in order to obtain a better understanding of the structure and dynamics of the hot plasma filaments that are observed in recent tokamak experiments. Simulation results show that the fast heating generates MHD waves and creates a localised hot filament. Pressure perturbations are carried away from the heated area by slow waves, even when the heating is applied on the Alfvén time scale. When a temperature-dependent resistivity is considered, a current peak is formed at the place of the temperature peak, and the order of magnitude of the current is given by the condition that ηJ_z is constant. Next to the wave dynamics, the simulations show another type of hot filament dynamics caused by $\mathbf{j} \times \mathbf{B}$ forces. These forces drive filaments to the centre of the plasma at a nearly constant velocity, which decreases for smaller resistivities. Two filaments can merge under the influence of this current–current interaction. This process happens on a very long time scale. For realistic tokamak resistivities, the coalescence of filaments may take place on time scales of the order of the experimentally reported lifetime of filaments, and may thus be the mechanism that determines the lifetime of the filamentation process.

1. Introduction

Recent tokamak experiments in the RTP tokamak of the FOM–Institute for Plasma Physics, The Netherlands, show that plasma filaments can exist in the centre of an externally heated plasma (Lopes Cardozo 1994; Lopes Cardozo *et al.* 1994; Box *et al.* 1995). During and after electron cyclotron heating (ECH), high and narrow peaks in the electron temperature occur in the plasma centre. Since it is believed that this filamentary structure of the plasma may account for anomalous effects in transport coefficients, it is important to try to understand these phenomena.

1.1. Open questions on filaments

The nature of the plasma filaments is still very unclear, and many questions on the interpretation of these phenomena remain open. These questions can be divided into three classes.

First of all, it is not clear by which mechanism the filaments form. Sometimes thermal instabilities are proposed as a possible explanation for filamentation of plasmas (Haines and Marsh 1982). It is also unknown whether the heating really creates the filaments, or just heats them up and makes them visible.

A second class of questions addresses the physical properties and structure of plasma filaments. What exactly do they look like? Do the observed temperature peaks go along with current peaks, and how do the pressure and the density behave at the location of a filament? The temperature peaks observed in the above experiments are called 'hot filaments'. They are believed to go along with pressure peaks, but they might also to some extent be related to (small) density depressions. The hot filaments are sometimes interpreted as closed flux tubes, and it is believed that they act as current channels, related to the fact that the plasma resistivity is expected to be lower at places of high temperature (Lopes Cadozo *et al.* 1994). However, such current filaments have not yet been measured. One of the reasons for the lack of knowledge on these points is that the present measurements are only one-dimensional and give only information on electron density and temperature, and not on current or magnetic field.

A third class of questions deals with the lifetime and the dynamics of the filaments. How long do they live, and how do they interact? Direct information on the lifetime and the interaction of filaments is very scarce. Thomson-scattering measurements at the RTP tokamak allow for only one or, since very recently, two measurements per plasma discharge. The temporal resolution of measurements is thus still very low.

Measurements in different but similar plasma discharges show that filaments in an EC-heated plasma still exist up to 500 μs after switching off the heating (Lopes Cardozo *et al.* 1994). This leads to the conclusion that the filamentation process has at least this lifetime. But it is not clear at all whether individual filaments exist for such a long time, or, on the contrary, that they continuously interact and mix, and maybe get regenerated by a kind of instability. Only measurements with a higher time resolution can address this question. Even the most recent state-of-the-art diagnostics in the RTP tokamak allow for only two measurements in one plasma discharge. The first results from these experiments (Beurskens *et al.* 1996) confirm that filaments continue to exist for a time of 100 μs. But it is still unclear whether individual filaments exist for such a long time or whether they interact.

1.2. Our model

In the present paper we want to address questions belonging to the second and third of the above classes, namely on the structure, lifetime and interactions of plasma filaments in a tokamak environment. We study these questions in the framework of the equations of resistive magnetohydrodynamics (MHD), which are solved numerically in two spatial dimensions. We investigate the reaction of a a tokamak-like equilibrium plasma state to a sudden localized deposition of heat. We shall call the resulting stationary temperature peaks 'hot filaments'. It is investigated how the temperature perturbations go along with changes in pressure, density and current, and on which time scales the resulting hot filaments 'stay alive'. We expect two fundamentally different types of dynamics in this problem. First, the strong perturbations of the plasma equilibrium induce nonlinear MHD waves. Secondly, two or more current peaks will dynamically interact, driven by the $\mathbf{j} \times \mathbf{B}$ force. We study both of these types of dynamics, and their influence on filament motion and

lifetime. This study of the dynamical behaviour of temperature perturbations imposed on a tokamak-like plasma equilibrium in the framework of 2D resistive MHD is a first approach to the problem of the dynamical behaviour of hot filaments as they are observed in tokamak experiments.

2. Filaments in the RTP tokamak

In this section we describe the parameters of the RTP tokamak and the experimental evidence for the existence of filamentation as reported in Lopes Cardozo *et al.* (1994).

The RTP tokamak has a major radius $R = 0.72$ m, and a minor radius $a = 0.16$ m. The toroidal magnetic field $B_T \leqslant 2.3$ T and the plasma current $I_p \leqslant 150$ kA. The safety factor $q_a \geqslant 2$ and $kT_e \approx 1$ keV (or $T_e \approx 1.2 \times 10^7$ K). The typical plasma density and pressure are $n_e = 3.0 \times 10^{19}$ m^{-3}, $\rho = 5.0 \times 10^{-8}$ kg m^{-3} and $p = 9.6 \times 10^3$ J m^{-3}. For a typical plasma the diameter of the $q < 1$ region is about 0.065 m. For $B = 2.0$ T these parameters give a value of 0.6% for the plasma β.

In a plasma with operating characteristics close to those mentioned above, filamentation was reported when ECH was used. If ECH is applied centrally, there is one big filament in the centre of the plasma. But when the heating is applied off-axis, many filaments are observed. All these filaments are found inside the $q = 1$ surface. Within this region the T_e profiles are characterized by several peaks. The n_e profiles also contain disturbances, but they are smaller and it is not clear if individual peaks in the temperature are correlated with individual disturbances in the density. The largest temperature peaks correspond to a temperature increase of about 50–75%, and the pressure peaks resulting from a combination of temperature and density measurements using the ideal gas law show a maximum pressure increase of about 75–100%. The width of individual filaments is between 5 mm and 10 mm.

The measurements do not give much information on the dynamics of the filaments. The electron temperature can only be measured once per plasma discharge. Information on the dynamics of the filamentation process can then be obtained by T_e measurements at different times for very similar discharges. In this way, it was measured that the plasma is still filamented up to 500 μs after switching off the ECH. Recent measurements with double-pulse Thomson scattering (Beurskens *et al.* 1996) allow for two measurements in one plasma discharge, with a possible time resolution of $10 - 20$ μs. These measurements will be able to give some information on the dynamics of the filaments.

It is clear that many questions remain open on the nature and the dynamics of plasma filaments. Are the electron pressure and temperature peaks strongly correlated in space and does this correlation remain intact for a long time? What is the relation of hot filaments to current peaks? Do the filaments interact, or do they keep their identity as individual objects for a long (≈ 500 μs) time?

3. The theoretical model: MHD dynamics of hot filaments

3.1. The theoretical framework: MHD

To describe the dynamics of filaments in a tokamak plasma, we use the nonlinear equations of compressible resistive one-fluid MHD, which read, in conservation

form,

$$\frac{\partial}{\partial t}\begin{bmatrix}\rho\\ \rho\,\mathbf{v}\\ \mathbf{B}\\ \mathscr{E}\end{bmatrix}+\boldsymbol{\nabla}\cdot\begin{bmatrix}\rho\,\mathbf{v}\\ \rho\,\mathbf{v}\mathbf{v}+\mathbf{I}(p+\frac{1}{2}\mathbf{B}\cdot\mathbf{B})-\mathbf{B}\mathbf{B}\\ \mathbf{v}\mathbf{B}-\mathbf{B}\mathbf{v}\\ (\mathscr{E}+p+\frac{1}{2}\mathbf{B}\cdot\mathbf{B})\mathbf{v}-(\mathbf{v}\cdot\mathbf{B})\mathbf{B}+\eta\,\mathbf{j}\times\mathbf{B}\end{bmatrix}=\begin{bmatrix}0\\ 0\\ -\boldsymbol{\nabla}\times(\eta\,\mathbf{j})\\ S\end{bmatrix}. \tag{1}$$

Here ρ and p are the plasma density and pressure respectively, $\mathbf{v}$ is the plasma velocity, $\mathbf{B}$ the magnetic field, $\mathbf{j}=\boldsymbol{\nabla}\times\mathbf{B}$ is the current density, and

$$\mathscr{E}=\frac{p}{\gamma-1}+\rho\,\frac{\mathbf{v}\cdot\mathbf{v}}{2}+\frac{\mathbf{B}\cdot\mathbf{B}}{2} \tag{2}$$

is the total energy density of the plasma. η is the plasma resistivity, S is an external heating source to be specified later, and $\mathbf{I}$ is the unit matrix. These equations have been made non-dimensional ($\mu=1$ in non-dimensional units, see below).

The plasma resistivity is modelled following the classical Spitzer formula (Priest 1982, p. 79)

$$\eta=\frac{c_{\mathrm{res}}}{T^{3/2}}\ , \tag{3}$$

with c_{res} a constant that will be specified later. In the ideal MHD simulations we take the resistivity equal to 0. For the equation of state we take the ideal gas law.

3.2. A model for the RTP plasma equilibrium

In our numerical simulations we shall impose a sudden localized deposition of heat on a static plasma equilibrium in a tokamak. We model the tokamak plasma as a periodic cylinder and consider a 2D azimuthal slice of this cylinder. The plasma equilibrium in this circular domain is modelled using a particular realization of the class of tokamak-like current profiles (TCP) (Wesson 1987, p. 143), which describe 1D cylindrically symmetric ideal MHD equilibria. In dimensionless units we take

$$B_z=1\ ,$$

and assume that the equilibrium current density and poloidal magnetic field are given by

$$J_z=J_{z,\mathrm{eq}}=J_0\,(1-r^2)^{\alpha}\ , \tag{4}$$

$$B_\theta=\frac{J_0}{2r\,(\alpha+1)}[1-(1-r^2)^{\alpha+1}]\ , \tag{5}$$

with $r\in[0,1]$. We take $\alpha=4$. The pressure then follows from the equations for a static equilibrium:

$$p=\tfrac{1}{10}J_0^2\,(\tfrac{1}{10}x^{10}+\tfrac{1}{12}x^{12}+\tfrac{1}{14}x^{14}+\tfrac{1}{16}x^{16}+\tfrac{1}{18}x^{18}) \tag{6}$$

where $x^2=1-r^2$. Choosing $q(0)=0.9$ and using

$$q(1)=\frac{aB_z(1)}{RB_\theta(1)}=(\alpha+1)\,q(0)\ ,$$

we get $q(1)=4.5$, $J_0=0.49$ and $p(0)=0.009$. We choose $\rho(0)=1$, and determine the density profile, which is a free profile in the ideal equilibrium, from the condition

$$\eta J_z=\mathrm{const}, \tag{7}$$

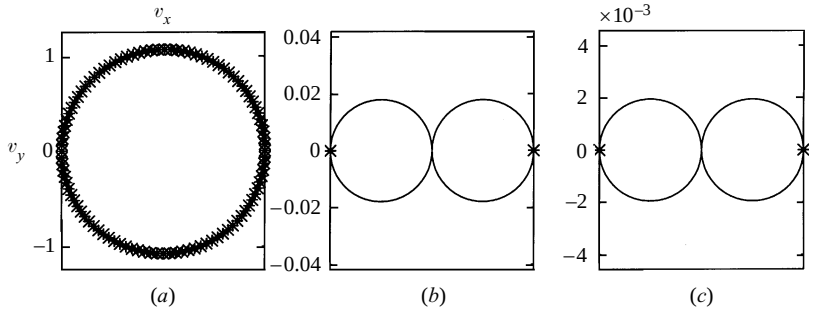

Figure 1. The directional dependences of the phase velocities (solid lines) and group velocities (asterisks) in the (x, y)-plane of the fast (a), Alfvén (b) and slow (c) MHD waves for the plasma state at position ($r = 0.18$, $\theta = 0$) of the plasma equilibrium (the v_x axis has the same scale as the v_y axis). The magnetic field has components in the x and z directions. For the fast wave, both the phase and group velocities are fairly isotropic. For the Alfvén and slow waves, the phase velocity and especially the group velocity are highly anisotropic. So we only expect Alfvén and slow waves propagating parallel to the projected magnetic field.

which leads to

$$T = c_T \, J_z^{2/3} \tag{8}$$

(with $c_T = 0.0144$), from which the density follows by the ideal gas law. In this way the equilibrium state is fully determined in dimensionless units. The condition (7) is assumed because it ensures that an ideal equilibrium will initially also be a resistive equilibrium for the induction equation, because the curl of $\eta \mathbf{j}$ vanishes in this case.

To check if these equilibrium values are a good approximation of RTP parameters during a typical plasma discharge in which filaments are detected, we have to convert the non-dimensional values back to physical values and compare with the RTP parameters as given in Sec. 2. We choose $\rho(0) = 5.0 \times 10^{-8}$ kg m^{-3}, $r = a = 0.16$ m and $B_z = 2.0$ T. Using $\mu = 4\pi \times 10^{-7}$ C m^{-2} and $\mathscr{R} = 1.65 \times 10^4$ J kg^{-1} K^{-1}, we find that $T(0) = 3.5 \times 10^7$ K, $p(0) = 2.9 \times 10^4$ J m^{-3} and $J_z(0) = 4.9 \times 10^6$ A m^{-2} (or $I_p = 79$ kA). The diameter of the $q = 1$ region is about 67 mm, and the plasma β is $\beta(0) = 1.8\,\%$. These values are close enough to the real RTP values given in Sec. 2 to expect typical behaviour in our numerical simulations that is comparable to the real plasma situation in RTP.

In a hyperbolic system a perturbation of an equilibrium will generate waves. In the MHD system three types of waves exist: the fast magnetosonic wave, the Alfvén wave and the slow magnetosonic wave. The Alfvén and slow waves are very anisotropic with respect to the direction of the magnetic field. The fast wave is almost isotropic and propagates in all directions. The slow and Alfvén waves propagate mainly parallel to the magnetic field, as can be seen in Fig. 1. In our plasma equilibrium the field lines of the projected magnetic field are concentric circles. From the general properties of the MHD waves we anticipate that the slow and Alfvén waves generated by perturbations will mainly propagate circularly, whereas the fast waves will propagate in all directions.

3.3. The numerical method

The equations (1) are solved numerically using a modern conservative high-resolution numerical scheme based on Godunov's method and an approximate linear

Riemann solver, as implemented in the numerical code EMMA_D. This code is based on a general approach for the numerical solution of hyperbolic conservation laws (Leveque 1992), which has proved to be highly successful in the field of computational fluid dynamics (Manna 1992), because of its accuracy, low artificial dissipation and good shock-capturing properties.

However, two main problems with the particular structure of the MHD conservation laws have prevented the application of these powerful techniques to the MHD equations until recently. The first problem, the numerical unstability related to the $\boldsymbol{\nabla} \cdot \mathbf{B} = 0$ constraint, was solved in Powell (1994) by the addition of an extra source term. The second problem, related to the degeneracy of the eigenvectors of the Jacobian under certain circumstances, was solved in Roe and Balsara (1996). Once these problems had been cleared, this technique started to be applied to astrophysical plasma flows (Gombosi *et al.* 1994).

The EMMA_D code uses a finite-volume discretization on a two-dimensional, structured, non-Cartesian grid. The fluxes through the cell interfaces are calculated using Roe's approximate linear Riemann solver (Roe and Balsara 1996). In this way, a basic explicit numerical scheme is obtained which is first order accurate in space and time. The scheme is enhanced to second order in space using slope-limited linear reconstruction at the cell interfaces. The limiter (a minmod limiter is used) guarantees that non-physical oscillations will not be generated. Second-order accuracy in time is obtained by a two-stage Runge–Kutta integration. The $\boldsymbol{\nabla}\cdot\mathbf{B} = 0$ related numerical instability is countered by the addition of Powell's source term, but it was found that, for the filametation simulations that we performed, this is insufficient to keep $\boldsymbol{\nabla} \cdot \mathbf{B}$ small enough, so an iterative projection scheme was added that solves a Poisson equation to a required accuracy. Non-ideal terms like resistivity are discretized separately in extra resistive fluxes and source terms. Boundary conditions are implemented using ghost cells.

This approach results in a highly accurate numerical scheme with good shock-capturing properties, low numerical diffusion and without spurious oscillations. Mass, momentum, magnetic field and total energy are conserved to a very high degree of accuracy. The EMMA_D code has been thoroughly tested on various test cases.

A numerical approach like this also has limitations. As we use an explicit time integration method, the timestep is limited by the condition

$$\Delta t \leqslant \frac{\Delta x}{|\lambda|_{\max}} \tag{9}$$

to keep the scheme numerically stable. In this condition Δx is the grid size in one dimension and λ is any wave speed in the hyperbolic system (fast, Alfvén or slow speed for MHD). Because the timestep has to be taken so small, we cannot always carry out computations to all physical times that are relevant, owing to limited computer resources. In our non-dimensional units, one unit of time ($t = 1$) corresponds to a physical time of 0.02 μs. In Fig. 1 we see that the fast waves have a non-dimensional speed of order 1, which means that fast wave dynamics will occur on a time scale of $t = 1$ (0.02 μs). Alfvén waves will propagate with a speed of about 0.05, which means a time scale of $t = 20$ (0.4 μs), and slow waves have a characteristic speed of about 0.005, with a time scale of $t = 200$ (4 μs). Owing to limited computer resources, the integration time on a 60×60 grid was limited to $t = 20$ (0.4 μs), which needed 40 000 explicit integration steps and 30 h of

CPU time on a fast workstation. On a 40×40 grid we did simulations until $t = 40$ (0.8 μs). These times are obviously far away from the stability times of 100 μs and 500 μs reported in experiments. The simulation results will show however that on these small time scales interesting dynamical behaviour occurs. Further integration in time needs more computer power or better numerical techniques. Performance could be improved using (semi)implicit methods on parallel computers.

A second limitation is the presence of numerical resistivity, which prevents us from taking the physical resistivity as low as required for a real tokamak situation. Using a convergence study in grid size and magnitude of the physically imposed resistivity, we were able to estimate the global numerical resistivity for our problem as $\eta_{\text{num}} = 3.5 \times 10^{-6}$ for the 60×60 grid and $\eta_{\text{num}} = 8 \times 10^{-6}$ for the 40×40 grid. The actual resistivity (3) put into the equations has to be substantially higher than the numerical resistivity. We chose $c_{\text{res}} = 0.5 \times 10^{-6}$ in (3), which gives $\eta = 3 \times 10^{-4}$ for a dimensionless temperature of $T = 0.014$ (which was the maximum temperature occurring in our simulations). This resistivity is clearly higher than the typical resistivity we expect in a tokamak ($\eta \sim 10^{-6} - 10^{-8}$). This high resistivity results in a diffusion that is faster than in reality: the magnetic energy is dissipated into internal energy, resulting in a decrease of the current and an increase of the temperature over the entire simulation domain. On the time scale on which we integrate, this effect is not too severe. However, if one wants to integrate further in time, the resistivity has to be lowered to avoid too much diffusion of the current. This can only be done by decreasing the numerical resistivity, and thus by taking a finer grid. However, this finer grid once again increases the burden on computer resources.

The numerical grid used in most of the simulations that are discussed in this article was generated using a grid relaxation procedure, resulting in the grid shown in Fig. 2. We remark that the computational cells near the four 'corners' of the domain are rather strongly deformed. This will lead to higher discretization errors near these points, so small errors will be present on the contour plots of simulation results in Figs 3, 5 and 10 below. However, these errors remain small even after 40 000 timesteps, and do not influence the solution in the more central part of the simulation domain, where the dynamics take place. Another disadvantage of the use of this type of deformed structured grid is that, for contour plotting with standard graphical packages, the values have to be interpolated onto a regular grid. This causes some irregularities in the contour closest to the circular external boundary. The highly deformed cells at the corner points also cause a higher interpolation error in those regions. These effects can be seen in Figs 3, 5 and 10.

The simulations are performed in a circular domain with an ideal wall at the boundary. This ideal wall boundary condition is imposed by mirroring (relative to the boundary edges) the magnetic and velocity field into the ghost cells, which makes the normal components of the fields equal to zero on the boundary edges, and by copying the density and energy from the first physical cell layer to the adjacent ghost cells.

The phase speed of the fast MHD wave goes to infinity when the density goes to zero. At the boundary $r = 1$ of our ideal MHD tokamak equilibrium, the density vanishes and the fast-wave speed becomes singular. Equation (9) shows that the timestep of our simulations will become too small then. To avoid this numerical difficulty we chose to carry out all the simulations on a domain bounded by $r = 0.5$. This does not put too many physical constraints on our simulations, because the

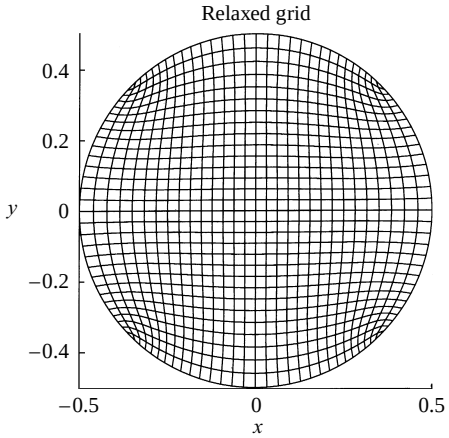

Figure 2. The simulation grid, obtained via a grid relaxation procedure.

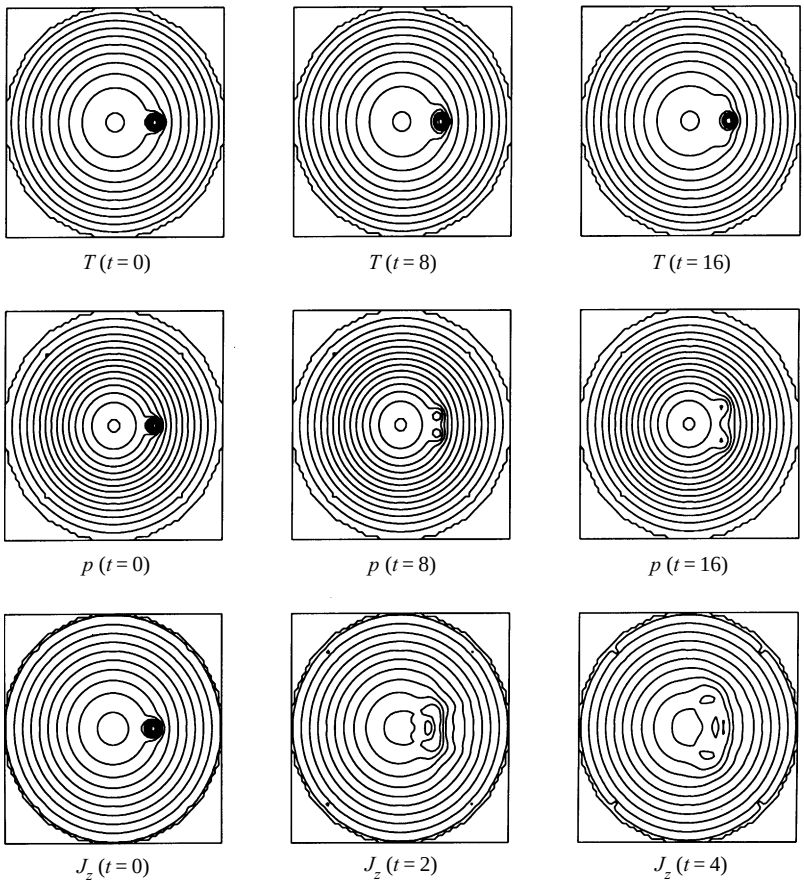

Figure 3. Filament of type A. Contour plots in time of the temperature, pressure and current. Ideal MHD on a 60×60 grid ($x, y \in [-0.5, 0.5]$).

filamentation we want to study is mainly concentrated in the centre of the plasma. So for all simulations we put the ideal wall at $r = 0.5$. The current at this boundary is kept fixed to the initial current at this location.

3.4. Models for a plasma filament

We shall consider four different types of initial conditions for a plasma filament, and label them A, B, C and D.

The results from the tokamak experiments on filamentation inspire us to look for a filament model with a localized peak in temperature and pressure, and we expect a current peak at the place of high temperature. As a first model for a hot filament (type A), we start by superposing an exponential current peak on the above mentioned tokamak plasma equilibrium. The current peak is modelled as

$$\begin{aligned} J_{z,\mathrm{fil}} &= a_J \ \exp\left(- \frac{r^2}{s^2} \right) , \\ J_{z,\mathrm{tot}} &= J_{z,\mathrm{eq}} + J_{z,\mathrm{fil}} \ , \end{aligned} \tag{10}$$

associated with a superposed magnetic field

$$B_\theta = \frac{a_J \, s^2}{2\, r} \left[1 - \exp\left(- \frac{r^2}{s^2} \right) \right] . \tag{11}$$

Typically we take $s = 0.025$, which leads to a current peak with a width of 8 mm. We use the condition

$$\eta J_{z,\mathrm{tot}} = \mathrm{const.} \tag{12}$$

to arrive at a perturbed temperature

$$T = c_T J_{z,\mathrm{tot}}^{3/2} \ , \tag{13}$$

ensuring the initial equilibrium of the resistive induction equation. This temperature perturbation can be thought of as an instantaneous localized deposition of heat. The density is taken equal to the equilibrium profile, resulting in a pressure peak at the place of the temperature and current peak. If we take $a_J = J_0$, the temperature and pressure peaks exceed the local equilibrium values by a factor of about 75%, close to the experimentally reported values of Sec. 2. The resulting initial condition for a filament of type A is plotted on the top row of Fig. 4 below.

In the course of our simulations we found the need for other initial conditions to model a hot filament. Filaments of type B have no initial current peak. Now the temperature has a Gaussian perturbation

$$T_{\mathrm{tot}} = T_{\mathrm{eq}} \left[1 + a_T \ \exp\left(- \frac{r^2}{s^2} \right) \right] , \tag{14}$$

with $s = 0.025$. Again the density is taken equal to the equilibrium density, which gives the pressure a peak at the place of the temperature peak. We took $a_T = 0.75$, which results in pressure and temperature peaks that exceed the local equilibrium values by a factor of about 75%. The resulting initial condition for a filament of type *B* is plotted in the third row of Fig. 4.

A filament of type C is generated starting from an initial condition that has no

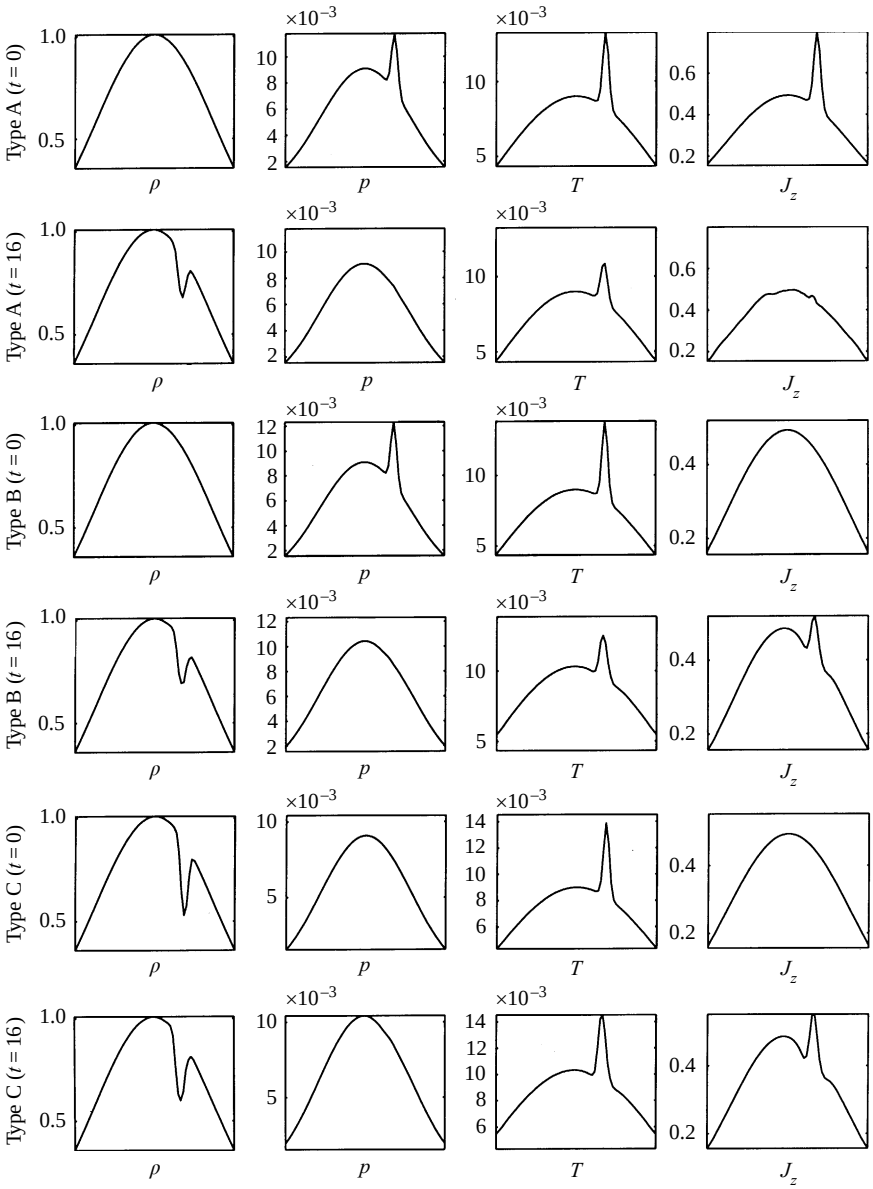

Figure 4. Initial conditions and plasma state at $t = 16$ for filaments of types A, B and C ($x \in [-0.5, 0.5]$, $y = 0$).

current peak (as in type B). Contrary to a type B filament, we now impose an initial density dip in stead of a pressure peak. So the temperature disturbance is taken as in (14), but the pressure is taken equal to the equilibrium pressure. The initial condition for a filament of type C is plotted in the fifth row of Fig. 4.

A last type of filament (type D) is generated via a localized heat deposition in time through the term S in (1). We start from the initial equilibrium and heating is applied during a given heating time interval, after which the heating is switched off. The heating is applied locally using the same Gaussian profile in space as in

Table 1. Comparison of the typical RTP and filament parameters with the simulation parameters.

	RTP	Simulations
R	0.72 m	∞
a	0.16 m	0.16 m
B_T	$\leqslant 2.3$ T	2.0 T
I_p	$\leqslant 150$ kA	79 kA
q_a	$\geqslant 2$	4.5
T	1.2×10^7 K	3.5×10^7 K
n_e	3.0×10^{19} m^{-3}	3.0×10^{19} m^{-3}
ρ	5.0×10^{-8} kg m^{-3}	5.0×10^{-8} kg m^{-3}
p	9.6×10^3 J m^{-3}	2.9×10^4 J m^{-3}
$d_{q<1}$	0.065 m	0.067 m
β	0.6%	1.8%
Filament width	5–10 mm	8 mm
ΔT_{fil}	50–75%	75%
Δp_{fil}	75-100%	75%

(10), resulting in

$$S = a_S \exp\left(-\frac{r^2}{s^2} \right) . \tag{15}$$

The value of a_S is chosen such that it will approximately double the energy $\mathscr{E}$ during the heating time. The initial energy $\mathscr{E}_0 = 0.0135$, so for a heating time of 20 we take $a_S = 0.000\,675$.

In this way we have models for filaments in which a given temperature peak initially goes along with a pressure peak (types A and B), with a density depression instead of a pressure peak (type C), or with both (type D).

In Table 1 we compare the physical RTP and filament parameters with the simulation parameters. We see that the simulation parameters are very close to the real RTP parameters, so we expect that the results of our dynamical simulations will be at least qualitatively relevant for a real RTP tokamak configuration.

3.5. Limitations of our model

First of all, the MHD model reduces the motion of the individual plasma particles to an averaged fluid motion, where for instance the influence of charge-separation forces is neglected. But this restriction is not too severe for our purposes, because MHD is a good model for the description of macroscopic plasma phenomena, and the observed filaments are of a macroscopic nature. Moreover, the MHD model is one of the few tractable models that describe dynamic interactions in plasmas.

Another limitation of our model is the reduction to two spatial dimensions. Although a sheared magnetic field is present in the considered tokamak plasma equilibrium, the influence of this shear on the plasma motions is a purely 3D effect. The 2D model cannot account for the special role of a 'transport barrier' that the $q = 1$ surface seems to play in real tokamak experiments (Lopes Cardozo *et al.* 1994). Numerical simulations in 3D, however, are much more complicated and computationally intensive than 2D simulations, so we have chosen for a 2D model as a first approach to the problem of the dynamics of filaments in a tokamak. As the simulation results will show, our 2D model contains enough physics to be able to draw

interesting conclusions about this problem. 3D simulations will be the subject of future work.

A third limitation of our approach is that we study the behaviour of perturbations of a plasma equilibrium, whereas the observed filaments could rather be plasma structures almost in equilibrium with the plasma environment. The MHD dynamics of a superposition of such close-to-equilibrium filaments will also be the subject of further work.

Although we are aware of its limitations, we use the 2D MHD model to initiate the study of the dynamics of hot filaments in a tokamak plasma. The numerical simulations give an idea about which types of filaments and interactions are possible. We hope that this gives indications for the interpretation of future measurements of filamentation phenomena with a higher time resolution.

3.6. Single-helicity models, full 3D calculations and toroidal effects

In this subsection we shall describe how we shall extend our code in the future to be able to do 2D single-helicity calculations and full 3D calculations in toroidal geometry. First we shall discuss how we expect the simulation results to be influenced by considering helical filaments and by taking toroidal effects into account.

3.6.1. Physical role of helicity, transport and toroidal effects. In vacuum two wires that carry currents of the same sign will attract each other. Intuitively, it can be expected that current filaments in a tokamak plasma will attract each other in a similar way. In the 2D calculations of this paper we show that this is indeed the case, and that this process may determine the lifetime of the experimentally observed filamentation process. This constitutes the physical relevance of the simulations described in this article. The basic effect of this attraction of current filaments may also be expected in a real 3D tokamak experiment. Our 2D model with planar symmetry allows for the basic mechanism of attraction between current filaments, but we can extend it by considering helical symmetry and by taking toroidal effects into account. Complications will arise in 3D from filaments that are not completely parallel to each other. These effects may add new dynamics to the behaviour of filaments in a tokamak. This will be investigated in forthcoming papers, and our present 2D calculations in cylindrical geometry with planar symmetry will serve as a reference for this future work.

Physically, 2D calculations with planar symmetry, 2D calculations with helical symmetry (the so-called 'single-helicity' approximation, using helical coordinates with a fixed helicity) and full 3D calculations (all in cylindrical geometry) are related in the following way.

Generally, only those inhomogeneities (or perturbations) in a plasma that are perpendicular to the magnetic field lines are important, because all inhomogeneities along the field lines tend to be wiped out very rapidly by the transport along the magnetic field lines, which is much more efficient than perpendicular transport (e.g. $\kappa_{\mathrm{par}} \gg \kappa_{\mathrm{perp}}$ for the heat-conduction coefficient). For numerical simulations, this means that ideally we have to choose an initial configuration with inhomogeneities perpendicular to the magnetic field lines, and that we have to conserve this property during the nonlinear evolution in time. In 2D simulations (with planar symmetry) of a tomamak plasma that has a q profile, such an initial configuration can only be modelled approximately (in our simulations the z component of the magnetic field is dominant, so the initial perturbations are almost perpendicular to the magnetic

field lines). A first improvement on this would be to consider 2D simulations in the single-helicity approximation. In this way one could specify a perturbation that is initially perpendicular to the magnetic field lines of this fixed helicity. These simulations would add a new aspect by allowing for helical filaments, instead of straight filaments. However, this approach is not yet completely satisfactory for the following three reasons. First of all, a typical tokamak equilibrium has a q profile, so different field lines have different helicities. By taking $q = 1$ for the helical coordinates, one could perhaps describe the influence of the $q = 1$ transport barrier, but the other helicities would not be treated properly. Secondly, in these strongly nonlinear calculations with large amplitude perturbations, the originally helical background field is changed substantially, so, after a while, the helical coordinates will no longer guarantee that the inhomogeneity will be perpendicular to the field! Thirdly, experiments show that the filaments (like islands) are highly localized in the toroidal (and helical) direction, so the inhomogeneities exist apparently also along the helical direction (precisely because the background field does not simply lie in a set of nested flux surfaces with given helicities, but is instead highly unhelical because of the presence of the filaments!). So we have to conclude that transport considerations can only be taken into account fully consistently in 3D calculations (with anisotropic heat conduction included in the model, to keep the perturbations perpendicular to the field lines during the nonlinear evolution of the plasma). This, however, is computationally a formidable task (even in the MHD model, compared with kinetic models, which are even more complex).

In these future simulations we shall also include toroidal effects, both in the 2D simulations (by introducing axial symmetry around the axis of the tokamak torus, both for planar symmetry and single helicity calculations), and in the 3D simulations.

3.6.2. Single-helicity models and 3D calculations. We shall extend our 2D code to be able to treat single-helicity symmetry in the following way. As in Rosenbluth *et al.* (1976) we define helical coordinates (subscript h) as

$$\left.\begin{aligned} r_h &= r, \\ \theta_h &= \theta - q\,z, \\ z_h &= z, \end{aligned}\right\} \tag{16}$$

where q is a constant. Instead of the planar symmetry $\partial/\partial z = 0$, we impose helical symmetry $\partial/\partial z_h = 0$, which leads to $\partial/\partial z = -q\,\partial/\partial\theta_h$. This means that in the ideal MHD equations (1) we have to include an extra source term. For the resistive part we have to include this term also in the derivation of the current from the field, and we have to make some adjustments in the treatment of $\boldsymbol{\nabla}\cdot\mathbf{B} = 0$ in Powell's source term and in the projection scheme.

Another approach to single-helicity calculations would be to use a 3D pseudospectral code with finite-difference discretization in the radial direction and Fourier decomposition in the other directions. A 2D single-helicity calculation can be performed by restricting the calculations to the ($n = 0$, $m = 0$) mode (which would describe the initial background equilibrium) and all modes of a given helicity. (See Poedts and Goedbloed (1997) for details.)

3D calculations can be done, if sufficient computer power is available, by extending the 2D finite-volume code to 3D. Proper modelling of some 3D physical effects (like ergodic field lines) may require adjustments to the numerical schemes. Proba-

bly an implicit time integrator and parallel computing would bring 3D simulations closer to reality.

4. Simulation results: nature and lifetime of one filament

In this section we describe the results of simulations in which we study the MHD behaviour of a sudden localized deposition of heat imposed on the plasma equilibrium, leading to a 'hot filament' (we recall that we call a localized temperature peak a 'hot filament'). We start with ideal MHD simulations of a filament of type A, with an initial current perturbation. Then we turn to resistive MHD simulations of types B and C filaments, where the current perturbation is not imposed initially, but is generated by a temperature-dependent resistivity. Finally, we create the hot filament using an external heating source (type D).

4.1. Ideal MHD of a hot filament

We put the initial condition for a filament of type A (perturbed temperature, pressure and current, the top row of Fig. 4) onto the plasma equilibrium, at the position $r = 0.18$, $\theta = 0$ (θ is the counterclockwise angle with the positive x-axis). This point is close to the $q = 1$ surface, just inside it. In Fig. 3 we show contour plots of the temperature, pressure and current evolution in time. The second row of Fig. 4 plots the plasma state on the x axis at time $t = 16$.

The temperature evolution in Fig. 3 shows that the temperature perturbation remains partially at the initial location, so a hot filament is formed by the perturbation. The other part of the temperature perturbation is carried away by a slow wave in the two directions along the projected magnetic field. The presure peak is carried away completely by this same slow wave. For several reasons it is clear that this wave is of the slow type. It clearly propagates along the magnetic field lines, so we conclude from Fig. 1 that it can only be an Alfvén wave or a slow wave, because only these waves have a group velocity (almost) completely along the magnetic field. If we look at the propagation speed of the pressure wave in Fig. 3, and compare it with the wave speeds of Fig. 1, we conclude that it can only be a slow wave. Also, it is known that Alfvén waves do not carry pressure perturbations.

The current peak in Fig. 3 is carried away by an Alfvén wave in the two directions along the projected magnetic field. This wave is clearly much faster than the slow pressure wave. It has a velocity of the order of the Alfvén-wave speed of Fig. 1, and it could be expected that magnetic perturbations are carried away by the Alfvén-wave mode.

We remark that we also observed fast waves in our simulations, which propagated from the perturbation isotropically in all directions, as is to be expected from Fig. 1. These fast waves, however, have a very small amplitude compared with the amplitudes of the Alfvén and slow waves and of the stationary peaks. They are damped out very rapidly by numerical resistivity and by numerous not completely perfect reflections at the ideal wall, so they are not observed on the time and magnitude scales of Fig. 3. (We also have to remark that these wave modes are not pure fast, Alfvén and slow modes, because of the nonlinear coupling and the non-homogeneous background. However, the wavelength of our perturbations is smaller than the characteristic scale of the plasma equilibrium, and this guarantees that the waves have properties close to the properties of the pure modes, so we shall call them fast, Alfvén and slow waves anyway.)

We can easily estimate the magnitude of the stationary part of the temperature perturbation. In ideal MHD the entropy is conserved, as is expressed by

$$\frac{d}{dt}\left(\frac{p}{\rho^\gamma}\right) = 0 \ . \tag{17}$$

At the location of the perturbation, we know from symmetry that the velocity will remain almost zero, so

$$\frac{\partial}{\partial t}\left(\frac{T^\gamma}{p^{\gamma-1}}\right) \approx 0 \ , \tag{18}$$

$$\left(\frac{T^\gamma}{p^{\gamma-1}}\right)_{\text{init}} \approx \left(\frac{T^\gamma}{p^{\gamma-1}}\right)_{\text{end}} \ . \tag{19}$$

For instance, in the top row of Fig. 4, we see that the intial temperature maximum is about $T_{\text{init}} = 0.014$, and $p_{\text{init}} = 0.012$. Since the pressure peak is carried away by a slow wave, and since the pressure relaxes to its equilibrium value at the place of the peak ($p = 0.007$), we can estimate from (19) that the remaining temperature peak has a height of $T = 0.011$. This is confirmed in the second row of Fig. 4.

We did some 1D and 2D simulations of a similar problem in hydrodynamics, without a magnetic field. Unfortunately we do not have enough room here to show the plots of the results. In 1D a temperature and pressure perturbation superposed on a constant background results in a sound wave that carries away the pressure peak and part of the temperature peak in two directions. The remaining temperature peak satisfies the relation (19). Because of the nonlinearity, the waves steepen. In 2D hydrodynamics the sound waves propagate in all directions. When a magnetic field is added, we get the three MHD wave types. We expect the fast wave to be almost isotropic, but the slow and Alfvén waves should propagate only along the magnetic field, so a perturbation should be carried away by them in the two directions along the magnetic field. The time evolution in Fig. 3 is fully consistent with these expectations.

The plasma state at the x axis after a (long) time $t = 16$ is plotted in the second row of Fig. 4. We see that a hot filament remains stationary. The pressure peak, however, is carried away completely by a slow wave. A stationary density dip is created. This is in contradiction with most of the experiments, where mostly the pressure is peaked at the location of a temperature peak, although filaments with pronounced density dips instead of pressure peaks have been observed as well. The current peak is taken away (almost) completely by an Alfvén wave. So we have to conclude that the model of a filament of type A in ideal MHD is rather far away from the picture of filaments we have from tokamak experiments and intuition, and hence, we have to improve our model. In Sec. 4.2 we shall try to arrive at a stationary current peak at the location of the temperature peak by including a temperature-dependent resistivity in our model. In Sec. 4.3 we shall try to create a stationary pressure peak by applying external heating.

4.2. Resistive MHD of a hot filament with an initial temperature perturbation

In these simulations we adopt the temperature-dependent resistivity (3), and investigate the behaviour of filaments of types B and C.

4.2.1. Hot filament with initial pressure perturbation. We impose the initial condition for a filament of type B (perturbed temperature and pressure; third row of Fig. 4)

onto the plasma equilibrium, at the position $r = 0.18$, $\theta = 0$. We do not impose an initial current perturbation derived from the condition (12), because we have seen in the ideal MHD simulations that this current perturbation is carried away along the magnetic field by Alfvén waves. (We have also tried this initial configuration (type A) in the resistive MHD model, with the same result.) So now we expect that the lower resistivity at the place of higher temperature will cause a redistribution of the current, resulting in a current peak at the place of the hot filament. In Fig. 5 we see that this is indeed the case: a current peak is formed at the place of the temperature peak. This current peak is not taken away by an Alfvén wave, and remains stationary at the position of the temperature peak. So in this model we are able to obtain a stationary hot filament with an associated current peak. The initial pressure peak, however, has the same behaviour as in the ideal MHD case, and is taken away by a slow wave. The resulting plasma state on the x axis at $t = 16$ can be seen in the fourth row of Fig. 4.

4.2.2. Hot filament with initial density perturbation. To see the effect of an initial density dip instead of an initial pressure peak, we investigate the evolution of a filament of type C, which we put again at $r = 0.018$, $\theta = 0$ (fifth row of Fig. 4). In Fig. 5 we see that a current peak is formed at the place of the temperature peak. The temperature peak remains almost completely in place, since there is no pressure perturbation and thus no slow wave to carry part of it away. Because the resulting stationary temperature peak is higher than in the previous case (type B), the resulting current will be higher. In the top row of Fig. 5 we see that the filament moves with a low, almost-constant speed towards the centre of the tokamak. We shall discuss this in more detail in Sec. 5.

4.2.3. Discussion. An interesting question is how high the current peak will be in relation to the temperature peak. It may be expected that the system of plasma equilibrium and perturbation will evolve to an equilibrium, in which case the condition (12) could be approached. In the bottom row of Figs 5 and 6, we plot the time evolution of the quantity ηJ_z. Initially the condition is far from fulfilled, because we did not impose an initial current peak. But the system clearly tries to approach this equilibrium, and in the initial evolution the big dip in ηJ_z is reduced very fast. But in the later evolution the relative magnitude of this dip seems to stabilize to a value of about 20–25% of the unperturbed ηJ_z value. (The profile is decreasing globally because of the resistive transfer of energy from magnetic energy to internal energy.) The fact that equilibrium is not fully attained could be related to the motion of the filament. In Sec. 5.1 we shall see that the filament moves with an almost-constant speed towards the centre of the plasma, as can already be seen from the plot of the plasma velocity in the top row of Fig. 6. For this constant motion of the filament, the moving plasma has to slip through the background magnetic field, and this slipping is exactly described by the $\eta \mathbf{j}$ term in the induction equation, so it is not a big surprise that ηJ_z does not relax to a constant.

So we can conclude that, from our simulations, we expect that a current peak will be present if there is a temperature peak and a temperature-dependent resistivity. The order of magnitude of the current peak can be estimated from the condition (12). However, in the simulations it seems to be lower by a factor of 20% or more, probably owing to the motion of the filament.

In this section we have shown that by incorporating a temperature-dependent

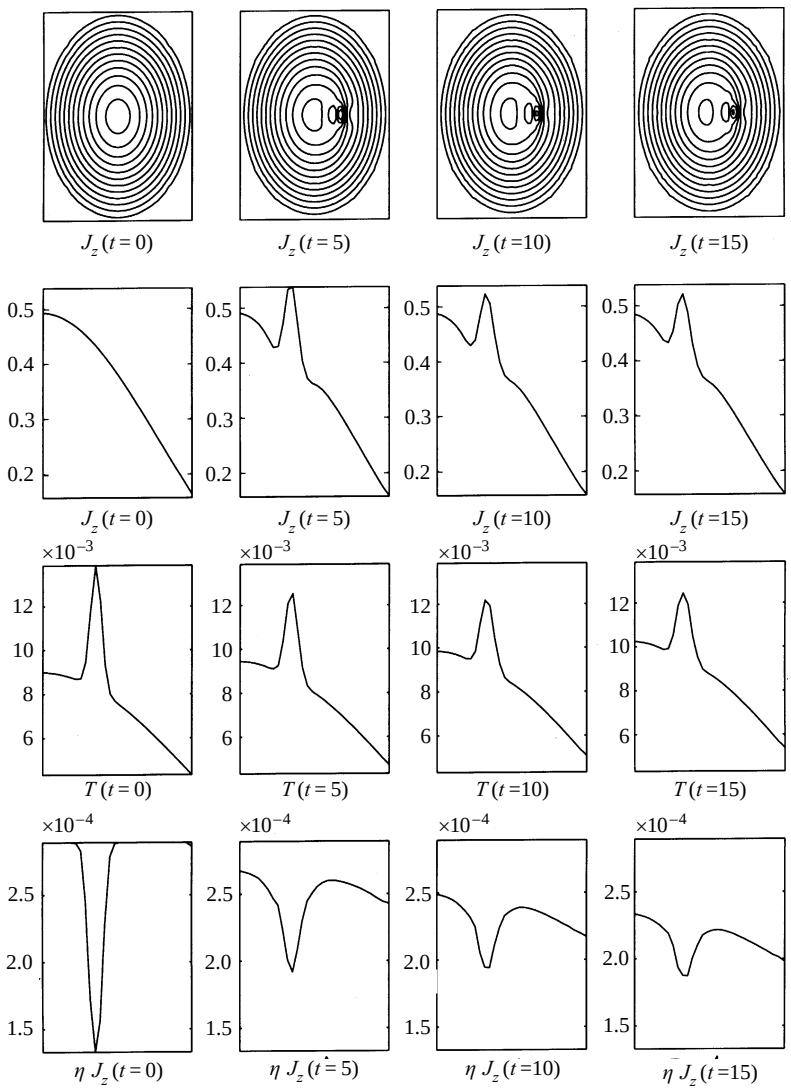

Figure 5. Filament of type B. Contour plot in time of the current ($x, y \in [-0.5, 0.5]$). Plots of current, temperature and ηJ_z ($x \in [0, 0.5]$, $y = 0$). Resistive MHD on a 60×60 grid.

resistivity in our model, we can create a stationary temperature filament with an associated current peak. The pressure perturbation however is still not yet stationary, but is taken away by a slow wave. In the next section we shall try to produce a stationary pressure filament using an external heating source.

4.3. Resistive MHD of a hot filament generated by external heating

In these simulations we start from the plasma equilibrium, and apply external heating as described in Sec. 3.4 (type D filament). In Sec. 4.2 the heat was deposited instantaneously, which induces waves, as could be expected. Also, this type of instantaneous deposition of a temperature peak leaves us with the arbitrary choice of putting only a pressure perturbation (type B), or only a density perturbation (type C), or actually anything in between (as long as the ideal gas law is satisfied). By

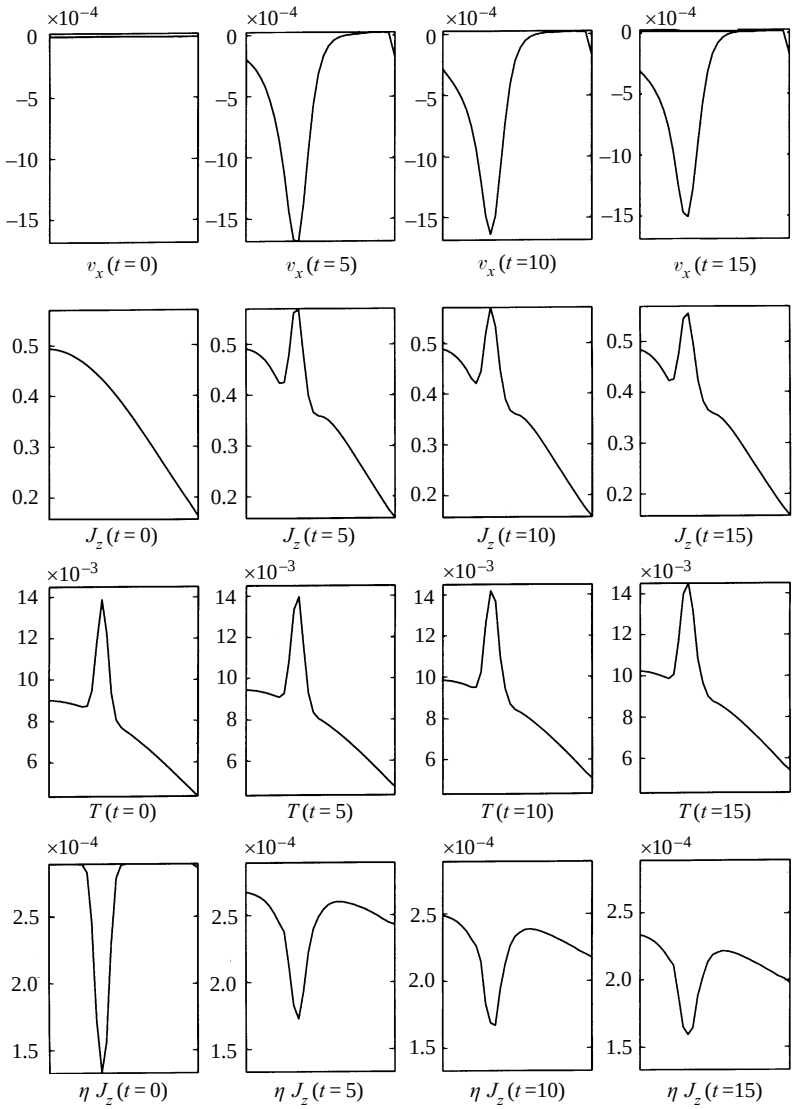

Figure 6. Filament of type C. Plots of x velocity, current, temperature and ηJ_z ($x \in [0, 0.5]$, $y = 0$). Resistive MHD on a 60×60 grid ($c_{\text{res}} = 0.5 \times 10^{-6}$).

applying gradual heating, density and pressure will both adapt at the same time in producing a temperature peak. It can also be speculated that by applying the heat slowly in time, the wave reaction will be less violent, and the magnetic field might have the time to adapt itself to a configuration in which it balances the ∇p force related to the induced pressure peak, by $\mathbf{j} \times \mathbf{B}$ action. So we hope to produce in this way a stationary temperature filament with an associated stationary pressure peak. The current peak will originate from a current redistribution as in the previous section, via a temperature-dependent resistivity.

In Fig. 7 we show some results of these simulations. External heating is applied from $t = 0$ till $t = 20$. We see that the temperature peak is formed by a perturbation

of both pressure and density. The associated current peak forms as expected. The pressure peak stays more or less located as long as heating is applied. However, when heating is put off, the pressure peak is (almost) completely taken away by a slow wave along the magnetic field. So external heating on this time scale does not create a stationary pressure peak. We have to note, however, that the heating time of 0.4 μs is much shorter than the actual heating times in an EC-heated plasma, and also much shorter than the time scale of the slow wave. Maybe much slower heating on this slow time scale could produce a stationary pressure peak. However, as explained in Sec. 3.3, with our numerical model and computer resources, we cannot carry out simulations that stretch that far in time. It is also possible that stationary pressure peaks cannot be produced by external heating in a 2D MHD model. This leads us to consider simulations in which we start from an initial configuration in which a pressure and magnetic field perturbation is present, such that $\mathbf{j} \times \mathbf{B} = \boldsymbol{\nabla} p$ and force equilibrium is present. Also, the 3D influence of the q profile might be important for the confinement of the pressure peak. Simulations incorporating these aspects will be the subject of future work.

The result that pressure that is deposited rather rapidly by external heating, is carried away by waves of a slow nature is an interesting result on its own, and prompts an experimental search for this kind of waves during and after external heating. To the best of our knowledge, there has not yet been a detailed search for this kind of waves in tokamak experiments.

In this section we have shown how we can produce stationary temperature filaments and associated current peaks in the model of 2D resistive MHD with a temperature-dependent resistivity. We have investigated the wave dynamics associated with the sudden deposition of heat in a tokamak plasma, and found that pressure peaks are carried away by slow waves and do not remain stationary even when they are generated by external heating on the Alfvén time scale.

In the next section we shall investigate the dynamics of these quasistationary filaments due to current–current interaction.

5. Simulation results: current–current interaction of hot filaments

It is well known that in vacuum two wires carrying a current in the same direction will attract each other with a force proportional to the product of the magnitudes of the two currents and inversely proportional to the distance between the wires. When several current peaks are present in a plasma, we expect that they will interact dynamically under the influence of this $\mathbf{j} \times \mathbf{B}$ force. This type of dynamics is fundamentally different from the wave dynamics discussed in Sec. 4. In this section we put several filaments of type C on the tokamak equilibrium, and we show how the $\mathbf{j} \times \mathbf{B}$ force leads to the motion of the hot filaments, and can cause filaments to merge.

5.1. Interaction of one filament with the equilibrium background current

In Fig. 8 we plot the results of a simulation in resistive MHD, where we put a filament of type C (initial temperature and density perturbation) on the plasma equilibrium. This is the same simulation as the one shown on Fig. 6, except for the value of the resistivity constant, which we choose 10 times larger here ($c_{\mathrm{res}} = 0.5 \times 10^{-5}$). In the top rows of Figs 6 and 8 we see that the plasma at the location of the temperature peak will move towards the centre of the simulation domain.

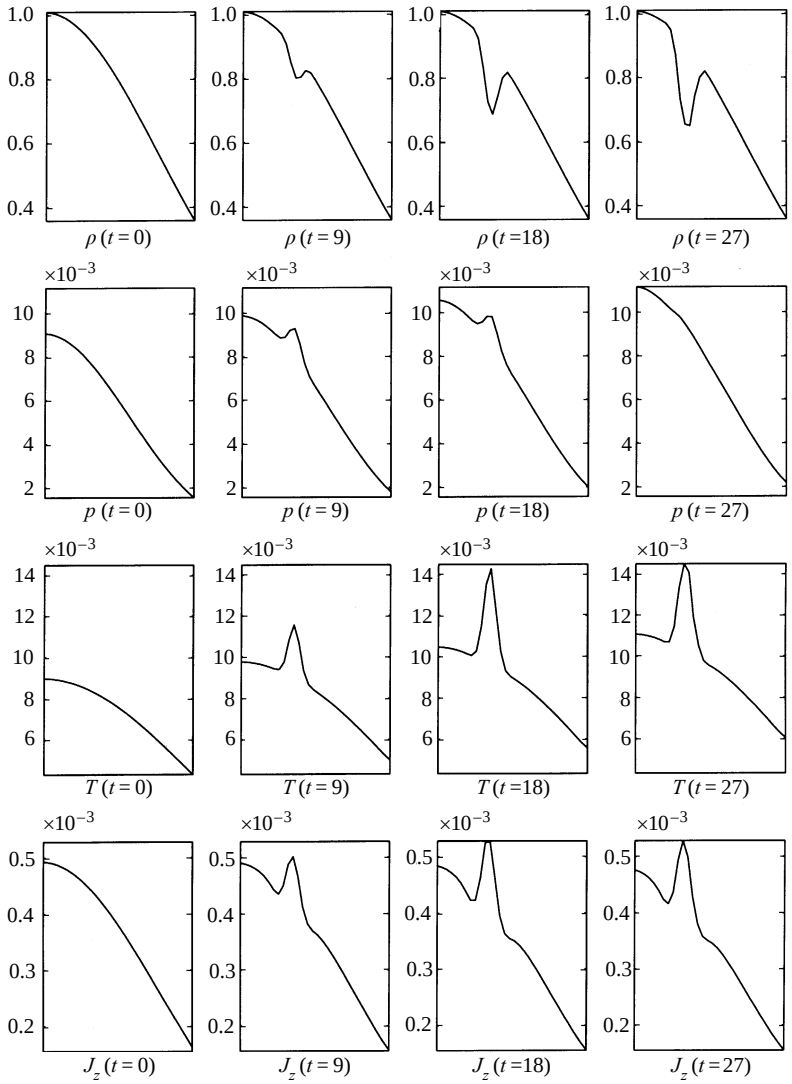

Figure 7. Filament of type D. Plots of density, pressure, temperature and current ($x \in [0, 0.5]$, $y = 0$). Resistive MHD on a 60×60 grid.

This behaviour can be explained as the attraction between the filament and the equilibrium background current. Detailed analysis of the simulation results shows that the temperature and current peaks move along with the plasma. The dynamics of the peak do not show an accelerated motion, so the $\mathbf{j} \times \mathbf{B}$ force on the plasma in the centre of the filament will be counteracted by the ∇p force. On the contrary, the velocity decreases slowly in time, as the filament approaches the centre. The velocity is slower than the slow characteristic speed, so these current–current interactions cause motions on a very long time scale.

The difference in resistivity of a factor 10 between the simulations in Figs 6 and 8 causes a difference in attraction speed by a factor of about 2.3. So lower resistivity leads to lower attraction speeds for the same temperature perturbation.

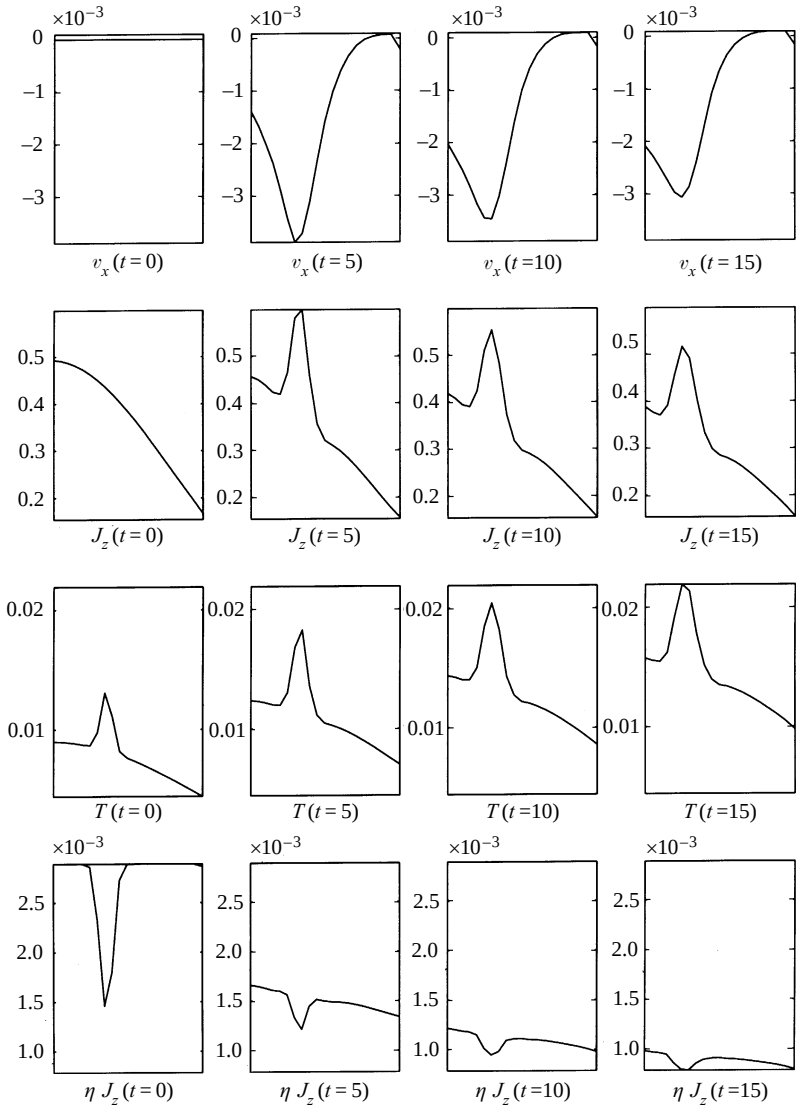

Figure 8. Filament of type C. Plots of x velocity, current, temperature and ηJ_z ($x \in [0, 0.5]$, $y = 0$). Resistive MHD on a 40×40 grid ($c_{\text{res}} = 0.5 \times 10^{-5}$).

It is not clear why this is so. It can be seen from the figures that higher resistivity causes a higher current peak relative to the current in the plasma centre, and this may lead to a higher velocity for the attractive motion. A more detailed parameter study is necessary to determine the exact relation between the magnitude of the resistivity, the magnitude of the temperature peak, the magnitude of the induced current peak and the velocity of the filament. It is also necessary to study in more detail how the background magnetic flux surfaces are deformed by the presence of the current peak, and how the hot plasma moves through the flux surfaces. This motion may involve field diffusion and reconnection at x-points. To investigate this process, higher-resolution simulations are required. It is possible that higher

resistivity allows for faster diffusion or reconnection, and thus faster movement of the hot filament through the flux surfaces. In any case, our results suggest already that for realistic tokamak magnetic Reynolds numbers, the attraction between current filaments leads to very slow motion. This may yield time scales of the order of the experimentally reported lifetime of 100 μs for this type of dynamic interaction. For instance, in the case of Sec. 4.2.2 ($c_{\text{res}} = 0.5 \times 10^{-6}$) a distance of $r = 0.1$ would be covered in about 1.5 μs. For realistic resitivities we should need $c_{\text{res}} = 10^{-10}$. As the attraction velocity decreases for a lower resistivity, this may lengthen the time scale of this interaction to experimentally reported time scales.

In Fig. 9 we show a vector plot of the total force $\mathbf{j} \times \mathbf{B} - \boldsymbol{\nabla} p$ and the velocity, superposed on contours of temperature and current respectively. We see that the force in the centre of the filament is very small, so the plasma is not accelerated there. At the right-hand side of the filament, plasma is accelerated from above and below, to fill in the density dip, so that the filament moves to the left. At the left-hand side plasma is accelerated towards the centre to create the density depression. These forces lead to a rather global flow of the plasma. The flow pattern does not seem to suggest that reconnection is taking place.

5.2. Interaction of two filaments with parallel current

In the top row of Fig. 10 we show how two filaments of type C (initial position $r = 0.18$, $\theta = \pm\frac{1}{6}\pi$) move towards each other and towards the centre ($c_{\text{res}} = 0.5 \times 10^{-5}$, resistive MHD). The velocity of attraction is small.

In the second row of Fig. 10 we put the two filaments of type C closer to each other (initial position $r = 0.18, \theta = \pm\frac{1}{18}\pi$), and see that two filaments can coalesce under the influence of this process. As our simulations suggest that, for realistic tokamak resistivities, this process may take place on time scales of the order of the experimentally reported lifetime of the filamentation process, the merging of filaments under the influence of $\mathbf{j} \times \mathbf{B}$ forces may be the mechanism that determines this lifetime.

5.3. Interaction of two filaments with antiparallel current

In the third row of Fig. 10 we show how two filaments of type C (initial position $r = 0.18$, $\theta = \pm\frac{1}{6}\pi$), but with antiparrallel current ($a_T = \pm 0.75$ in (14)), repel each other. The upper filament has a temperature and current depression, and moves away from the centre and from the lower filament, which has a temperature and current peak. The lower filament moves towards the plasma centre.

In this section we have made clear how the $\mathbf{j} \times \mathbf{B}$ forces cause an attractive motion of current filaments. This motion happens on a slow time scale, and gets even slower for lower resistivity. This motion can cause filaments to merge. We can speculate that for realistic resistivities the merging of filaments by this process may happen on the experimentally reported time scales of about 100 μs, and may thus determine the lifetime of the filamentation process.

6. Conclusions

In this paper we have investigated how the sudden localized deposition of heat on a 2D MHD tokamak plasma equilibrium leads to the generation of localised hot filaments and MHD waves. The hot filaments are accompanied by current

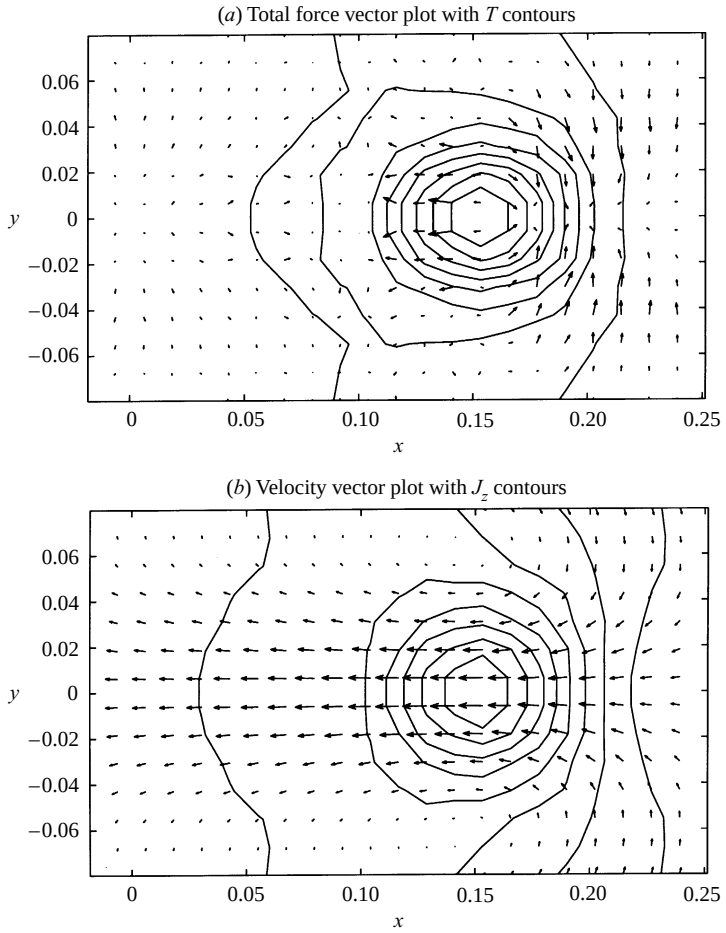

Figure 9. Filament of type C, with $c_{\mathrm{res}} = 0.5 \times 10^{-5}$, at $t = 10$. (*a*) Total force and temperature. (*b*) Plasma velocity and current.

filaments in the model of resistive MHD with a temperature-dependent resistivity. The current peaks undergo current–current interaction caused by the $\mathbf{j} \times \mathbf{B}$ force, and can merge under the influence of this force.

First we showed that instantaneous deposition of heat leads to a long-lived stationary hot filament. An initial current peturbation is carried away along the projected magnetic field by an Alfvén wave. Pressure perturbations are carried away along the magnetic field by slow waves, even when they are generated by external heating on the Alfvén time scale.

In the model of resistive MHD with a temperature-dependent resistivity, a current peak is created at the location of the hot filament as the background current is redistributed. The order of magnitude of this current peak can be derived from the condition $\eta J_z = \text{const}$. As time evolves, this equilibrium condition is approached, but equilibrium is not attained, probably owing to the motion of the hot filament.

Hot filaments in resistive MHD are shown to be influenced by $\mathbf{j} \times \mathbf{B}$ forces. Filaments move towards the centre of the plasma as they are attracted by the

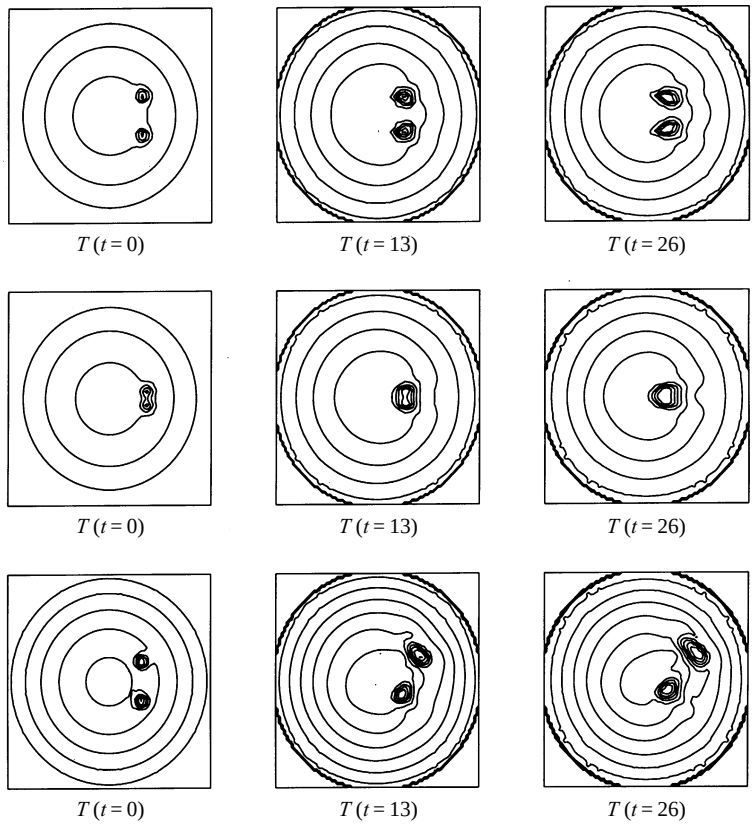

Figure 10. Temperature evolution of the current–current interaction of two filaments. Top row: filaments with parallel current attract each other. Middle row: coalescence of two filaments with parallel current. Bottom row: filaments with anti-parallel current repel each other. Resistive MHD on a 40×40 grid ($c_{\text{res}} = 0.5 \times 10^{-5}$, $x, y \in [-0.5, 0.5]$).

background current. The forces and flows adjust themselves such that this motion of the filament has an almost-constant speed. This speed is smaller than the slow characteristic speed, and decreases for decreasing resistivity. The temperature and current peaks are dragged along with the moving plasma. Two filaments with parallel current attract each other, and can merge under the influence of this attractive force. Two filaments with antiparallel currents repel each other. This current–current interaction happens on a very slow time scale, and it can be speculated that for realistic resistivities this process of merging filaments may take place on time scales of the order of the experimentally reported lifetime of filaments (100 μs), and may thus be the mechanism that determines the lifetime of the filamentation process.

Further investigations will have to clarify some of these points. A detailed parameter study has to determine the relation between the magnitude of the resistivity, the temperature peak, the current peak and the velocity of the moving filament. Simulations with higher resolution have to make clear how the magnetic flux surfaces are deformed by the presence of the current peak, how the hot filaments move through these flux surfaces by diffusion or reconnection, and how a difference in resistivity in these processes may cause a difference in the velocity of the

attractive motion. Only then can a reliable prediction be made for the time scale of the current–current interaction process with realistic resistivities. Next, a filament with a stationary pressure peak has to be constructed, and we must investigate how several filaments of this type interact. Finally, the influences of the q profile and the $q = 1$ surface, the helicity of filaments, and toroidal effects have to be accounted for in single helicity and 3D simulations in toroidal geometry. A problem of another nature is the origin of the filamentation process. Of course this problem is very important and interesting, and it deserves further investigation in the MHD model, or beyond. These points will be the subject of future research.

Acknowledgements

We thank M. Beurskens, N. J. Lopes Cardozo and the RTP team for useful input and discussions about the experimental aspects of filamentation in the RTP tokamak. We thank G. Tóth for interesting discussions on grid relaxation and MHD simulations, and B. C. Low for discussions on the concepts of helical and 3D calculations. H. De Sterck wants to thank the FOM-Institute for Plasma Physics for its kind hospitality during numerous visits, and for the use of computer facilities. H. De Sterck is a Research Assistant of the Fund for Scientific Research, Flanders, Belgium (FWO), and S. Poedts is a Research Associate of the FWO.

References

Beurskens M. N. A., Barth, C. J., Chu, C. C., Lopes Cardozo, N. J., van der Meiden, H. J., Pijper, F. J. and the RTP-team 1996 Double pulse Thomson scattering at RTP: first results. *Proceedings of the 23rd EPS Conference on Controlled Fusion and Plasma Physics, Kiev*, pp. 1088–1091.

Box, F. M. A., Beurskens M. N. A., Steenbakkers, M. F. M., Barth, C. J., Chu, C. C., Lopes Cardozo, N. J., Pijper, F. J., Westerhof, E. and the RTP-team 1995 Non-Maxwellian velocity distributions and spatial structures in electron temperature profiles of Ohmic and EC-heated discharges in RTP. *Proceedings of the 22nd EPS Conference on Controlled Fusion and Plasma Physics, Bournemouth*, Vol. 2, pp. 129–132.

Gombosi, T. I., Powell, K. G. and De Zeeuw, D. L. 1994 Axisymmetric modeling of cometary mass loading on an adaptively refined grid: MHD results. *J. Geophys. Res.* **99**, 21 525–21 539.

Haines, M. G. and Marsh, F. 1982 A steady-state model of current filamentation caused by the electrothermal instability in a fully ionized magnetized plasma. *J. Plasma Phys.* **27**, 427–435.

Leveque, R. J. 1992 *Numerical Methods for Conservation Laws. Lectures in Mathematics, ETH Zurich*. Birkhäuser, Basel.

Lopes Cardozo, N. J. 1994 Plasma filamentation in the Rijnhuizen tokamak RTP. *Phys. Rev. Lett.* **73**, 256.

Lopes Cardozo, N. J., Barth, C. J., Chu, C. C., Lok, J., Montvai, A. Oomens, A. A. M., Peters, M., Pijper, F. J., de Rover, M., Schuller, F. C., Steenbakkers, M. F. M. and the RTP-team 1994 Filamentation in tokamaks. *Proceedings of International Conference on Plasma Physics, Foz do Egaucu, Brasil*, pp. 81–88.

Manna, M. 1992 A three-dimensional high resolution compressible flow solver. PhD thesis, Université Catholique de Louvain.

Poedts, S. and Goedbloed, J. P. 1997 Nonlinear wave heating of solar coronal loops. *Astron. Astrophys.* **321**, 935–944.

Powell, K. G. 1994 An approximate Riemann solver for magnetohydrodynamics (that works in more than one dimension). Technical Report 94-24, ICASE Langley, VA, 1994.

Priest, E. R. 1982 *Solar Magnetohydrodynamics*. Reidel, Dordrecht.

Roe, P. L. and Balsara, D. S. 1996 Notes on the eigensystem of magnetohydrodynamics. *SIAM J. Appl. Maths* **56**, 57–67.

Rosenbluth, M. N., Monticello, D. A., Strauss, H. R. and White, R. B. 1976 Numerical studies of nonlinear evolution of kink modes in tokamaks. *Phys. Fluids* **19**, 1987.

Wesson, J. 1987 *Tokamaks*. Clarendon Press, Oxford.